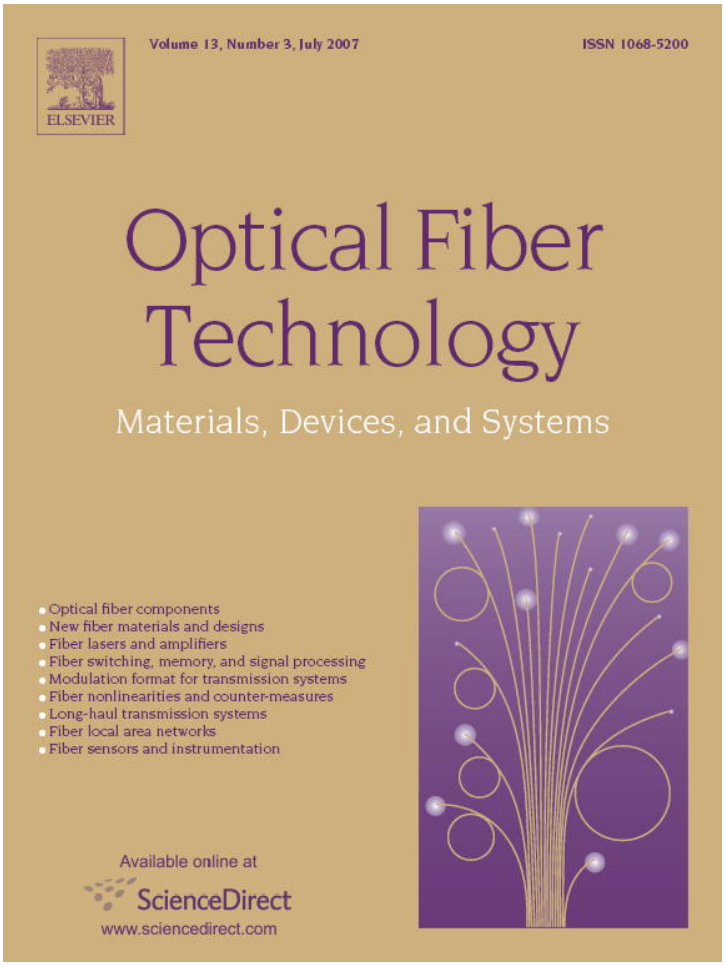

Available online at www.sciencedirect.com
ScienceDirect
Optical Fiber Technology 13 (2007) 240–245
Optical Fiber Technology
www.elsevier.com/locate/yofte

Optical phase-front inscription over optical fiber end for flexible control of beam propagation and beam pattern in free space

Jun Ki Kim [a,*], Yongmin Jung [a], Byeong Ha Lee [a], Kyunghwan Oh [c], Chaemin Chun [b], Dongyu Kim [b]

[a] *Department of Information and Communications, Gwangju Institute of Science and Technology, 1 Oryong-dong, Buk-gu, Gwangju 500-712, South Korea*
[b] *Department of Material Science and Engineering, Gwangju Institute of Science and Technology, 1 Oryong-dong, Buk-gu, Gwangju 500-712, South Korea*
[c] *Department of Physics, Yonsei University, 134 Shinchon-dong, Seodaemun-gu, Seoul 120-749, South Korea*

Received 5 June 2006; revised 23 November 2006

Available online 26 March 2007

Abstract

We report a novel compact all-fiber technique to control the beam propagation and beam pattern in free space. By coating an azo-polymer thin film layer on the optical fiber end surface, various surface relief grating (SRG) structures were inscribed over the film using a single step direct exposure of interference patterns to form a novel organic/inorganic composite fiber optics beam shape converter. The linear and concentric SRGs were experimental characterized along with numerical simulations.

Keywords: Optical phase-front; Beam shape controller; Beam transforming; Surface relief grating; Maskless lithography; Azo-polymer

1. Introduction

Beam transforming and the beam pattern control have been one of key issues in optical technologies and various techniques based on nonspherical lenses or other diffractive optical devices have been developed [1–3]. Waveguide-branching or phase-front matching using micro-prism have been main methods to control phase-front curvature or power distributions [4–6]. Prior beam reshaping and pattern engraving technique, however, relied mainly on the use of bulk optical system, which required complicated design and fabrication processes at the risk of surface damages.

Along with fast development in fiber optic communications and sensory systems, various attempts have been made to incorporate the bulk-optic technique into optical fibers. Mechanical deformation of fiber ends into spherical or wedge-shaped surfaces have been one of first attempt in fiber optics for applications in laser-diode to optical fiber coupling [7–9]. Reflowing of photoresist on the fiber ends have been also attempted utilizing conventional micro-lithography and etching techniques [10,11]. Laser direct writing of phase-fronts over endfaces of optical fibers has been reported, which can obviate substantial routines in lithographic technologies, yet it required sophisticated optical alignments and expensive femto-second laser systems. Recently the authors have proposed composite optical fibers with polymeric phase-front modification for beam forming [12,13] and beam pattern control [14], which showed strong potentials for flexible and economic optical phase-front control without resorting to conventional lithography and etching techniques.

In this paper, we report numerical simulation of the diffraction patters out of azo-polymer SRG on the fiber, and introduce a new method to inscribe concentric circular SRGs to manipulate the propagation properties of a beam. The principles, fabrication procedure, and characterization of beam propagation and beam patterns from linear and circular azo-polymer SRGs are discussed both experimentally and theoretically.

2. Formation of linear and concentric surface relief grating (SRG) on optical fiber end surface

Azo-polymer complexes have been widely used to inscribe periodic optical structures due to their unique mass shift in-

* Corresponding author.
E-mail address: jkkim@gist.ac.kr (J.K. Kim).

1068-5200/$ – see front matter
doi:10.1016/j.yofte.2007.02.003

duced by photo-reaction. It has been observed that exposing a thin film of azo-polymer to a light intensity gradient leads to spontaneous surface patterns. In essence, the polymer material will reversibly deform so as to minimize the amount of material exposed to the light. This phenomenon is not laser ablation, since it readily occurs at low power and the transformation is reversible. This exact mechanism of this surface holography is still unresolved, although it is clearly related to the azo-benzene isomerization [15]. The epoxy-based azo-polymer PDO3 was synthesized from diglycidyl ether of bisphenol A and 4-(4′-nitrophenylazo) phenyl amine for the experiments. Detailed syntheses of PDO3 were described elsewhere [16,17]. Compared to photoresist films, azo-polymer layers produce surface relief grating (SRG), where the actual mass of layer is modulated rather than refractive index by absorption of blue-green photons. In a single-step writing process, topographic structures on the azo-polymer layers can be formed upon exposure to the appropriate optical patterns [18,19]. This process, therefore, has a significant advantage over other techniques which typically involve multiple steps, such as baking, exposure and developing, etc.

Developing interferometric lithographic technology, we inscribed both linear and concentric phase-fronts over the azo-polymer layers on optical fibers to form surface relief gratings (SRGs) in a single exposure without using any photo-mask, or further post-processes. For the linear SRGs, we have used formation of linear fringe patterns using conventional two-beam interference setup based on bulk-optics. In contrast to these linear SRGs, we report a novel and compact fiber-optic pattern generator to inscribe circular concentric SRGs, for the first time to the best knowledge of the authors. The concentric interference pattern was generated within the cross section of the fiber, using a coreless fiber segment and adjusting its length.

For both linear and concentric SRGs, principal fabrication procedures can be divided into three main steps; fiber endface preparation, azo-polymer thin film coating, and optical pattern generation and exposure. Note that direct exposure of various phase-fronts over optical fiber is the unique advantage of the proposed technique, which could be readily applicable to both fiber arrays and planar waveguides providing strong economic mass production capability.

A single-mode optical fiber (Corning SMF-28) was, first, cleaved to form an optically flat endface, which makes a right angle with respect to the fiber axial direction, using an ultrasonic high precision fiber cleaver. The cleaved endface served as a substrate for azo-polymer thin film coating. PDO3 polymer containing azo-benzene group was solvated in cyclohexanone and the filtered 10 wt% PDO3 solution was dropped on the fiber-end-surface and then spin-coated. The film was, then, dried in a vacuum oven at 80 °C for 1 h. Due to relatively low viscosity of the solution, we could achieve azo-polymer thin film with flat and smooth surface. The thickness of the film in this study was 900 nm and had a flatness of ±20 nm over the entire circular optical fiber endface whose diameter was 125 μm.

Experimental setup for optical pattern generation and exposure is shown in Fig. 1 for both linear (a) and concentric (b, c).

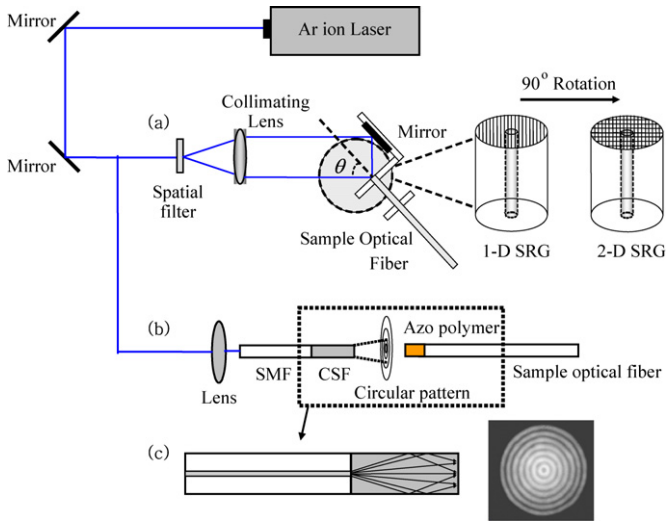

Fig. 1. Experimental setup for (a) linear and (b) concentric SRGs on the fiber-end-surface, (c) detailed schematics for generation of concentric interference patterns using composite fiber optic device. Photograph is the actual interference pattern at the end of coreless silica fiber (CSF).

Note that the proposed process is direct one-step exposure to generate SRGs obviating photo masks and etching processes. Schematic diagram for fabrication of linear SRGs is presented in Fig. 1a. An Ar-ion laser operated at 488 nm was used as a writing beam, whose intensity was 100 mW/cm^2. The laser output was expanded by a spatial filter and subsequently collimated by a lens. Linear interference patterns were formed due to optical path difference between the direct beam and reflected beam at the mirror. The pitch of interference was adjusted by changing the incident angle θ, which determined the period (Λ) of SRG pattern on azo-polymer film. To inscribe a uniform linear pattern with a pitch of 2 μm, the angle of incident was adjusted to 7°. Once the linear interference pattern was exposed to azo-polymer, one-dimensional SRG was formed by the mass-shift. Over the one-dimensional SRG, another pattern can be overlaid to form a two-dimensional SRG, whose detailed procedures have been reported in Ref. [14].

Figures 1b and 1c are the schematic diagram for concentric SRGs patterning. In contrast to the linear SRGs based on conventional bulk optics in Fig. 1a, concentric interference patterns were generated by a compact composite optical fiber device. The device was composed of single-mode fiber (SMF) and coreless silica fiber (CSF) concatenated by arc-fusion splice as shown in Fig. 1c. CSF does not have GeO_2 doped high index core and serves as a homogeneous propagation medium for the LP_{01} mode exiting from the SMF core. As the light exits from the SMF core, it passes through CSF, a homogeneous silica dielectric, expanding the beam diameter, which can be approximated by Gaussian beam propagation [12,13]. As the beam further propagates along CSF, part of the beam hits the air–glass interface, and then reflects into CSF, generating circular interference patterns. The pitches of circular interference patterns are controlled by the CSF length. For the CSF length of 900 μm and longer, a full concentric interference pattern was formed on the entire CSF cross-section, which was then used to engrave the circular patterns on the azo-polymer film on the

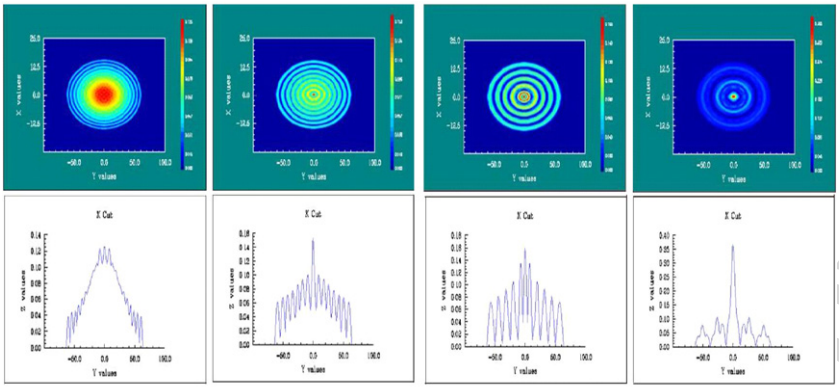

Fig. 2. The numerical estimation of the intensity distributions for various CSF lengths using a BPM simulation tool.

other fiber end as in Fig. 1b. The photograph on the right hand side of Fig. 1c is the actual near field image at the output of the proposed SMF-CSF composite device measured by a CCD camera, which clearly confirms generation of a concentric interference pattern. This concentric interference pattern is then projected to the sample optical fiber whose end face is coated with azo-polymer film. By the optical intensity contrast in the interference pattern, we can inscribe concentric SRGs over the azo-polymer film.

In order to further investigate the role of CSF length in the concentric interference pattern generation, we used a commercial beam propagation method (BPM) package, BeamPROP, for numerical analysis and the results are summarized in Fig. 2. Here we assumed the fundamental mode of SMF can be approximated as a Gaussian beam as it propagates along CSF, which has been widely accepted for calculation of light propagation in the free space out of SMF [20]. The outer diameters of both SMF and CSF were 125 μm. As shown in Fig. 2, the intensity distribution and fringe spacing were directly dependent on the CSF length for the given diameter. For the CSF length less than 700 μm, the beam pattern stays in Gaussian distribution without concentric fringes. As the CSF length approaches near 700 μm, fringe patterns appear overlaid on the Gaussian beam. For CSF length longer than 900 μm, the entire cross-section of CSF is filled with concentric interference fringes. As the CSF length increases furthermore, less numbers of fringes and longer pitch were predicted. Varying the geometrical dimension of CSF, diameter and segment length, therefore, the proposed composite fiber-optic device can provide very versatile and flexible control over the concentric interference pattern generation. As an external parameter we can also consider the distance between the CSF end face and azo-polymer end face, yet we but-coupled the two fiber ends in this study in order to isolate the role of CSF length in concentric SRG formation. Further investigation of circular pattern generation is being studied by the authors.

The scanning electron microscope (SEM) images of the fabricated SRGs are shown in Fig. 3. Two-dimensional linear SRG is shown in Fig. 3a. The bright center regions of the figures denote the location of the fiber core. First, one-dimensional (1-D) linear SRG was fabricated on the fiber-end-surface. The pitch was 2 μm and the modulation depth was in the range 450–500 nm. For this 1-D SRG, another linear interference pattern was exposed after rotating the fiber at an angle of 90 degrees from the initial position, to form two-dimensional (2-D) linear SRGs as in Fig. 1a. As a result of this double exposure, a 2-D SRG with 2 μm-by-2 μm periodicity was fabricated as shown in Fig. 3a. It is noted that the fundamental mode of SMF spread out to the entire cross-section of the fiber including both the core and cladding to result in effective modification of the phase front of incident beam, the LP_{01} mode guided by the SMF.

In concentric SRGs, on the while, we used the composite SMF-CSF pattern generators with the CSF lengths of 1000 and 1500 μm, and the SEM images of fabricated SRGs are shown in Figs. 3b and 3c, respectively. The pitches of the engraved concentric SRG patterns were about 2.7 and 4.3 μm for Figs. 3b and 3c, respectively. As numerically predicted in Fig. 2, we could experimentally confirm that the composite pattern generator with the CSF length of 1000 μm provided a concentric SRG with a larger number of fringes with a narrow pitch compared with those of 1500 μm CSF case.

Utilizing azo-polymer thin films over SMFs, we could experimentally confirm that direct exposure of both linear and concentric interference pattern at 488 nm Ar-ion laser can successfully form the corresponding SRGs

3. Measurements and simulations of diffraction patterns out of SRGs over optical fiber

The optical field propagating through the SMF will experiences the spatially periodic modulation provided by the SRGs at the prepared endface of the fiber, resulting in unique diffraction patterns. Fabricated SRGs on SMF were further examined in terms of their diffraction pattern both experimentally and theoretically. In order to investigate impact of the SRGs over beam patterns, the far-field diffraction patterns from the SRG on SMFs were measured by a CCD camera using a laser source at 635 nm.

In Fig. 4a, schematic diagram of the experimental setup for measurement of diffraction patterns is shown, where L is the distance from the SRG to the measured diffraction patterns,

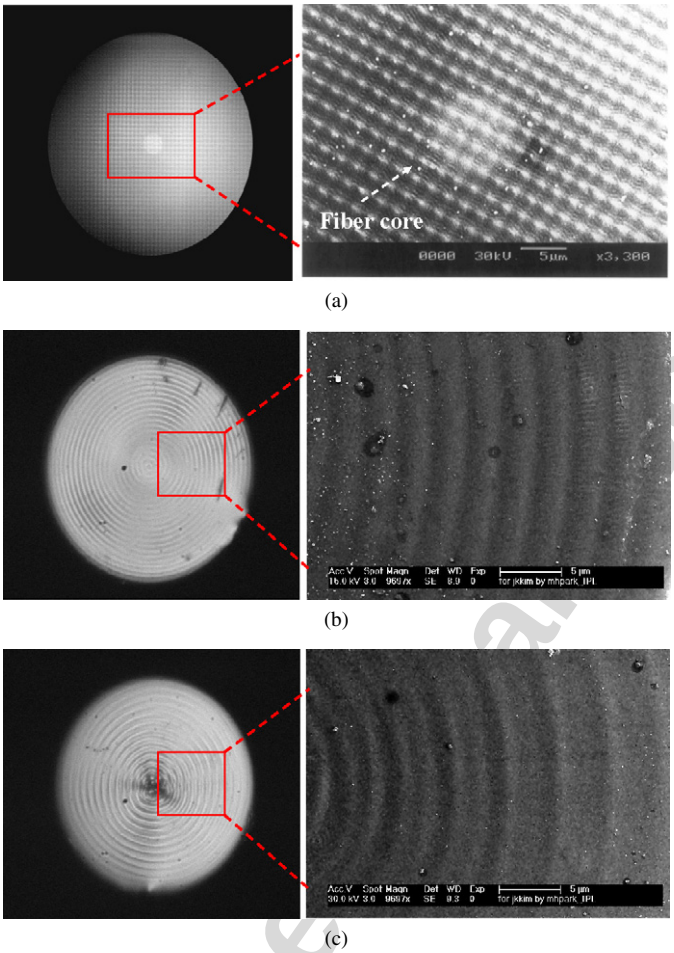

Fig. 3. SEM images on the fiber-end-surface with (a) 2-D linear SRG; $\Lambda = 2$ μm; (b) concentric SRG with the CSF length of 1000 μm, $\Lambda = 2.7$ μm; (c) concentric SRG with the CSF length of 1500 μm, $\Lambda = 4.3$ μm.

and D is the distance between the zeroth- and the first-order diffraction beam pattern, and θ_m is the diffraction angle. From the diffraction patterns, we can calculate the diffraction angle (θ_m) by measuring the distance data (D and L), and finally obtain the SRG pitch (Λ) from the following diffraction grating equation

$$\Lambda = m\lambda / \sin\theta_m, \tag{1}$$

where m denotes the order of principle maxima [21].

Measured diffraction patterns and the line profile for the case of linear SRGs is shown in Fig. 4b.

In Fig. 4b, clear diffraction beam pattern of the zeroth- and the first-order from the linear SRG was observed. The circular pattern at the center is identified as the zeroth-order and the four first-order side lobes perpendicular to one another, was measured as shown in Fig. 4b.

The far field diffractive patterns and the line profiles of the concentric SRGs are shown in Figs. 4c and 4d. Note that the orders of diffraction do differ for SRGs made of concentric pattern generators with the CSF lengths of 1000 and 1500 μm. For the case of CSF length of 1000 μm, the diffraction pattern has the central zeroth-order and one thin ring, which corresponds to first-order. In the case of 1500 μm CSF, we can clearly dissolve two rings, which correspond to first- and second-order diffraction, overlaid with the zeroth-order circular pattern. In comparison to diffraction patterns from linear SRGs, as in Fig. 4b, those from the concentric SRGs do not show clear and definitive images, which is attributed to relatively low contrast in the concentric interference pattern generators (see Figs. 2b and 2c). Minima of the fringes do have finite intensity and subsequently SRG would have shallow contrast to make the diffraction pattern less definitive. Further improvement in the contrast of the concentric interference patterns are being investigated by the authors.

Table 1
Measured data from diffraction pattern measurements

	L (mm)	D (mm)	θ (°)	Λ (μm) (calculated)	Λ (μm) (measured)
2-D linear SRG	10	3.39	18.73	1.98	2.0
CSRG with 1000 μm	11.68	3.0	14.41	2.55	2.7
CSRG with 1500 μm	19.11	3.0	8.92	4.10	4.3

The measured diffraction parameters are shown in Table 1, from which we calculated the pitches (Λ) of SRGs. For linear 2-D SRGs, pitches was calculated as 1.98 μm. For concentric SRGs made by the SMF-CSF interference pattern generators of CSF length of 1000 and 1500 μm, the pitches were calculated as 2.55 and 4.10 μm, respectively. Compared with pitches mea-

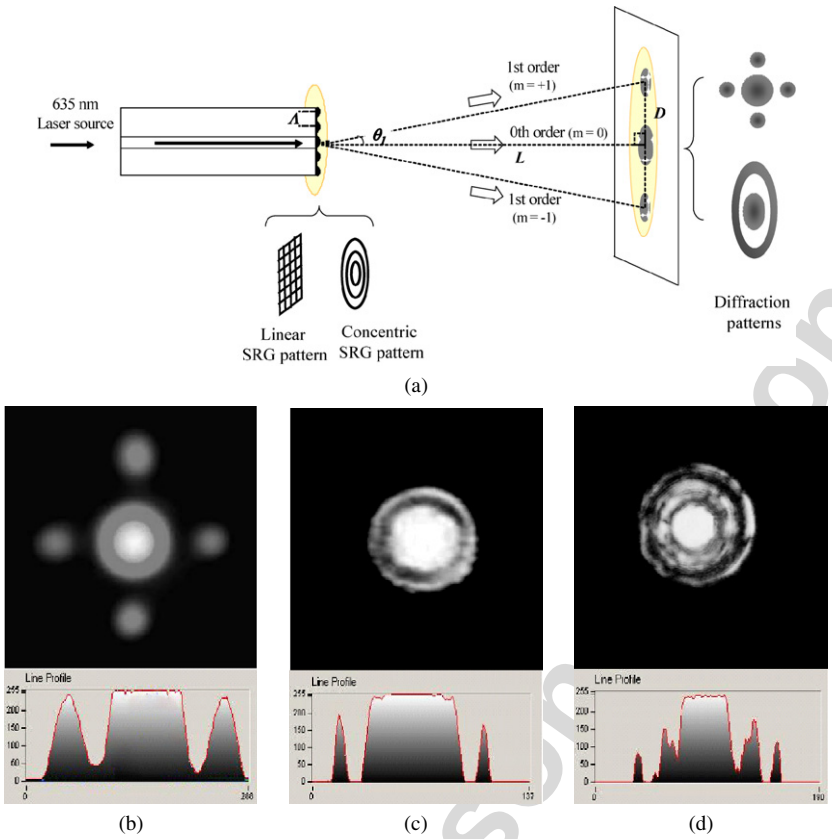

Fig. 4. (a) Schematic diagram of measuring diffraction beam patterns; diffraction beam patterns and line profiles of (b) 2-D linear SRG; (c) concentric SRG with the CSF length of 1000 μm; (d) concentric SRG with the CSF length of 1500 μm.

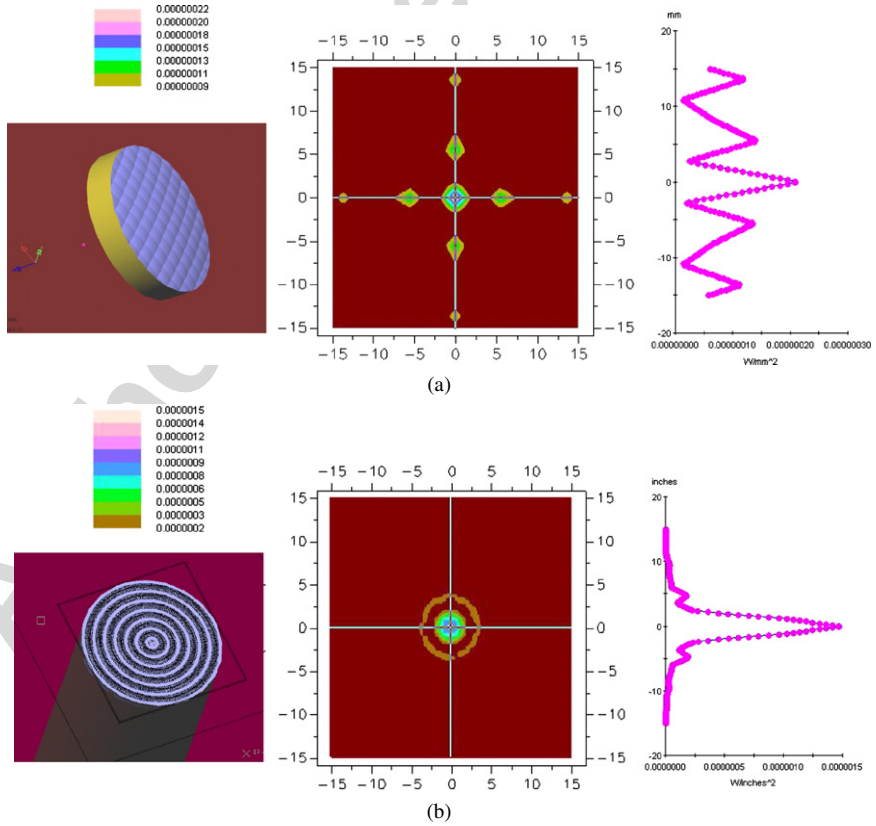

Fig. 5. The simulation results of the irradiance chart using LightTools; (a) irradiance chart of the linear surface relief grating and the linear grating template; (b) irradiance chart of the concentric surface relief grating and the circular grating template.

sured by SEM images in Fig. 3 in Section 2, these numbers are in a reasonably good agreement as summarized in the last two columns of Table 1.

Diffraction patterns from the fabricated SRGs on optical fiber endfaces were also theoretically investigated using a commercial simulation package, LightTools. In the simulation tool, the diffraction of the guided mode from the given SRG were investigated in terms of the irradiance beam patterns using the illumination analysis. Actual dimension of the SRGs were used in the simulation with an approximation that the incident light is Gaussian, instead of LP_{01} mode of the SMF, which is very common in the free space optic analysis. The illumination analysis in the LightTools is based on a Monte Carlo ray trace [22], which traces the desired number of rays from randomly selected points on the surface or volume into randomly selected angles in space. Diffraction patterns from the linear SRG, Fig. 3a, and concentric SRG, Fig. 3b, were simulated using the tool and the irradiance chart results are shown in Fig. 5. In comparison with experimental measurements, Figs. 4b and 4c, we could find the simulation results showed good agreement in terms of the line profiles, the intensity distribution along x- or y-axis, and diffraction robe locations.

Through these experimental and theoretical analyses, we could confirm that the proposed method to form SRGs on the optical fiber endfaces does have practical feasibility and can endow a new degree of freedom to design integrated optical systems compatible to fiber optics or waveguide optics. With this experimentally proven high potential, the technique can be applied to various kind integrated optical devices and systems such as beam splitter, beam deflector, diffractive lens, and beam shape controller for phased-array antenna.

4. Conclusions

Both linear and concentric surface relief gratings (SRGs) have been successfully inscribed on azo-benzene polymer thin film deposited over optical fiber endfaces by developing novel maskless lithography technology. Utilizing unique advantage of the azo-polymer such as direct writing and multiple exposure capabilities, various SRGs were flexibly designed and fabricated. For the case of linear 2-D SRGs, conventional two-beam interference patterns at 488 nm were used. A novel SMF-CSF concatenated device was proposed to generate concentric interference patterns whose intensity distribution can be further tailored by CSF length and area. Utilizing a Monte Carlo ray tracing package, diffraction pattern out of SRGs were simulated with a good agreement with experimental results. By this phase front inscription technology, we were able to control and manipulate the propagation properties of light in free space, which can find direct applications in integrated optical components and sub-systems for optical communications.

Acknowledgment

This work was supported in part by the KOSEF (Program Nos. R01-2006-000-11277-0 and R15-2004-024-00000-0) and the Scientific and Technological Cooperation program between Italy and South Korea from MOST, Korea.

References

[1] J.W. Ogland, Mirror system for uniform transformation in high power annular laser, Appl. Opt. 17 (1978) 2917–2923.
[2] D.F. Cornwee, Nonprojective transformation in optics, Opt. Eng. 294 (1982) 62–72.
[3] S. Kawakami, Light beam redistribution using computer generated phase plates, J. Lightwave Technol. 7 (1989) 1412–1418.
[4] H. Sasaki, Normalized power transmission in single-mode optical branching waveguides, Electron. Lett. 17 (1981) 136–138.
[5] W.Y. Hung, Novel design of wide angle single-mode symmetric Y-junctions, Electron. Lett. 24 (1988) 1184–1185.
[6] W.-C. Chang, A novel low-loss wide angle Y-branch with a diamond-like microprism, IEEE Photon. Technol. Lett. 11 (1999) 683–685.
[7] J. Sakai, T. Kimura, Design of a miniature lens for semiconductor laser to single-mode fiber coupling, J. Quant. Electron. 16 (1980) 1059.
[8] H. Yoda, K. Shiraishi, A new scheme of a lensed fiber employing a wedge-shaped graded index fiber tip for the coupling between high power laser diodes and single mode fibers, J. Lightwave Technol. 19 (2001) 1910.
[9] H. Ghafoori-Shiraz, T. Asano, Microlens for coupling a semiconductor laser to a single-mode fiber, Opt. Lett. 11 (1986) 537–539.
[10] L.G. Cohen, M.V. Schneider, Microlenses for coupling junction lasers to optical fibers, Appl. Opt. 13 (1974) 89–94.
[11] G. Eisenstein, D. Vitello, Chemically etched conical microlenses for coupling single-mode lasers into single-mode fibers, Appl. Opt. 21 (1989) 3470–3474.
[12] J. Kim, M. Han, S. Chang, W. Lee, K. Oh, Achievement of large spot size and long collimation length using UV curable self-assembled polymer lens on a beam expanding core-less silica fiber, IEEE Photon. Technol. Lett. 16 (11) (2004) 2499–2501.
[13] K.-R. Kim, S. Chang, K. Oh, Refractive microlens on fiber using UV-curable fluorinated acrylate polymer by surface-tension, IEEE Photon. Technol. Lett. 15 (8) (2003) 1100–1102.
[14] S. Choi, K.-R. Kim, K. Oh, Interferometric inscription of surface relief gratings on optical fiber using azo-polymer film, Appl. Phys. Lett. 83 (2003) 1080.
[15] H. Rau, in: J. Rebek (Ed.), Photochemistry and Photophysics, vol. 2, CRC Press, Boca Raton, FL, 1990, pp. 119–141.
[16] D.Y. Kim, L. Li, X.L. Jiang, V. Shivshankar, J. Kumar, S.K. Tripathy, Macromolecules 28 (1995) 8835.
[17] X. Wang, L. Li, J. Chen, S. Marturunkakul, J. Kumar, S.K. Tripathy, Macromolecules 30 (1997) 219.
[18] D.Y. Kim, et al., Laser-induced holographic surface relief gratings on nonlinear optical polymer films, Appl. Phys. Lett. 66 (1995) 1166.
[19] P. Rochon, E. Batalla, A. Natansohn, Optically induced surface gratings on azoaromatic polymer films, Appl. Phys. Lett. 66 (1995) 136.
[20] H. Kogelnik, On the propagation of Gaussian beams of light through lens-like media including those with a loss and gain variation, Appl. Opt. 4 (1965) 1562.
[21] E. Hecht, Optics, Addison–Wesley, San Francisco, 2002.
[22] M.J. Hayford, et al., Illumination Module User's Guide, Opt. Res. Assoc., 2003.